PERGAMON

International Journal of Heat and Mass Transfer 42 (1999) 4225–4233

International Journal of HEAT and MASS TRANSFER

www.elsevier.com/locate/ijhmt

Entropy generation due to laminar natural convection over a heated rotating cylinder

Bassam A.K. Abu-Hijleh*, Waleed N. Heilen

Mechanical Engineering Department, Jordan University of Science and Technology, PO Box 3030, Irbid 22110, Jordan

Received 26 June 1998

Abstract

Entropy generation due to laminar mixed convection from an isothermal rotating cylinder was calculated numerically. The study was conducted for three cylinder radii and covered wide ranges of Reynolds number and buoyancy parameter. Entropy generation increased as the Reynolds number and buoyancy parameter increased. Entropy generation decreased as the cylinder radius increased. For the same combination of Reynolds number and buoyancy parameter, entropy generation was mainly due to thermal effects at small cylinder radii and due to viscous effects at large cylinder radii. © 1999 Elsevier Science Ltd. All rights reserved.

1. Introduction

The optimal design criteria for thermal systems can be achieved by minimizing entropy generation in the systems. This problem has recently been the topic of great interest in fields such as heat exchangers, energy storage systems, and electronic cooling devices. Heat transfer processes are accompanied by thermodynamic irreversibility due to entropy generation. There exists a direct proportionality between the irreversibility of the process and the amount of useful work dissipated in the process. Entropy generation was studied by many investigators. Bejan [1] showed that the entropy generation for forced convective heat transfer is due to temperature gradient and viscosity effect in the fluid. San and Laven [2] investigated the irreversible entropy generation for combined heat and mass transfer in a two dimensional channel. Hutchinson and Lyke [3] used a lumped analysis to investigate entropy generation in regenerative heat exchangers. Different research on local entropy generation in heat exchangers is available in the literature [4–8].

Natural convection from a horizontal cylinder has been investigated extensively. Kuehn and Goldstein [9] numerically solved the complete Navier–Stokes and energy equation for laminar natural convection about a horizontal isothermal cylinder for $1 \leq Ra_D \leq 10^7$ using a finite difference technique. Wang et al. [10] investigated the laminar natural convection flow from a heated horizontal cylinder using the spline fractional step method. Ghaddar and Thiele [11] numerically solved natural convection over a rotating cylindrical heat source in a rectangular enclosure, using a finite element method. Shimada et al. [12] experimentally investigated the heat transfer from a rotating cylinder with and without cross flow. Badr [13] theoretically solved laminar mixed convection from a horizontal cylinder in cross stream. Badr et al. [14] numerically solved the steady and unsteady flow past a rotating circular cylinder at low Reynolds numbers. Ahmad [15] numerically solved steady state forced convection around a horizontal cylinder at moderate Reynolds numbers, ranging from 100 to 500. In the present work

* Corresponding author. Tel.: +962-2-295111; fax: +962-2-295018.

E-mail address: bassam@just.edu.jo (B.A.K. Abu-Hijleh)

0017-9310/99/$ - see front matter
PII: S0017-9310(99)00078-2

Nomenclature

D	cylinder diameter
Gr	Grashof number based on radius, $\equiv g\beta r_o^3(T_o-T_\infty)/\nu^2$
Gr_D	Grashof number based on diameter, $\equiv g\beta D^3(T_o-T_\infty)/\nu^2$
g	acceleration due to gravity
$\bar{h}$	average convection heat transfer coefficient
h	local convection heat transfer coefficient
k	thermal conductivity
M	number of grid points in the tangential direction
N	number of points in the radial direction
Nu_D	local Nusselt number based on diameter, $\equiv hD/k$
$\overline{Nu_D}$	average Nusselt number, $\equiv \bar{h}D/k$
p	pressure
p^*	normalized pressure
R	dimensionless radial distance, $\equiv r/r_o$
r	radial direction in computational domain
r_o	radius of the cylinder (m)
R_∞	dimensionless far away boundary distance, $\equiv r_\infty/r_o$
r_∞	faraway boundary distance
Ra_D	Rayleigh number based on diameter, $\equiv g\beta D^3(T_o-T_\infty)/\nu\alpha$
Re	Reynolds number based on radius, $\equiv r_o^2\Omega/\nu$
Re_D	Reynolds number based on diameter, $\equiv r_o\Omega D/\nu$
S_c	conduction contribution to dimensionless total entropy generation
S'''_{gen}	dimensionless local entropy generation
s'''_{gen}	entropy generation per unit volume (W/m^3 K)
S_t	dimensionless total entropy generation
S_v	viscous contribution to dimensionless total entropy generation
T	temperature
U	dimensionless radial velocity, $\equiv u/r_o\Omega$
u	radial velocity
V	dimensionless tangential velocity, $\equiv v/r_o\Omega$
v	tangential velocity

Greek symbols

α	thermal diffusivity
β	coefficient of thermal expansion
ϵ	relative error
η	radial direction in computational domain
θ	tangential direction in physical domain
κ	buoyancy parameter, $\equiv Gr_D/Re_D^2$
μ	dynamic viscosity
ν	kinematics viscosity
ξ	tangential direction in computational domain
ρ	density
ϕ	dimensionless temperature, $\equiv(T-T_\infty)/(T_o-T_\infty)$
ψ	dimensional stream function
ψ^*	dimensionless stream function, $\equiv\psi/r_o\Omega^2$
Ω	rotational speed
ω	dimensional vorticity
ω^*	dimensionless vorticity, $\equiv\omega/\Omega$

Subscripts

∞	ambient value
o	value on cylinder wall

the complete Navier–Stokes and energy equations are solved using finite difference technique to describe laminar natural convection over a heated rotating cylinder. The overall entropy generation rates around a rotating cylinder are calculated for different values of Reynolds number, buoyancy parameter and cylinder radius.

2. Mathematical analysis

Fig. 1 shows a schematic of the cylinder and the main physical parameters. The equations for steady state two-dimensional laminar mixed convection from a horizontal rotating cylinder are given by [16]:

$$\frac{1}{r}\frac{\partial(ru)}{\partial r}+\frac{1}{r}\frac{\partial v}{\partial\theta}=0 \tag{1}$$

$$u\frac{\partial u}{\partial r}+\frac{v}{r}\frac{\partial u}{\partial\theta}-\frac{v^2}{r}= -\frac{1}{\rho}\left[\rho g\beta(T-T_\infty)\cos(\theta)+\frac{\partial p}{\partial r}\right] +\nu\left[\frac{\partial^2 u}{\partial r^2}+\frac{1}{r}\frac{\partial u}{\partial r}-\frac{u}{r^2}+\frac{1}{r^2}\frac{\partial^2 u}{\partial\theta^2}-\frac{2}{r^2}\frac{\partial v}{\partial\theta}\right] \tag{2}$$

$$u\frac{\partial v}{\partial r}+\frac{v}{r}\frac{\partial v}{\partial\theta}+\frac{uv}{r}= \frac{1}{\rho}\left[\rho g\beta(T-T_\infty)\sin(\theta)-\frac{1}{r}\frac{\partial p}{\partial\theta}\right] +\nu\left[\frac{\partial^2 v}{\partial r^2}+\frac{1}{r}\frac{\partial v}{\partial r}-\frac{v}{r^2}+\frac{1}{r^2}\frac{\partial^2 v}{\partial\theta^2}+\frac{2}{r^2}\frac{\partial u}{\partial\theta}\right] \tag{3}$$

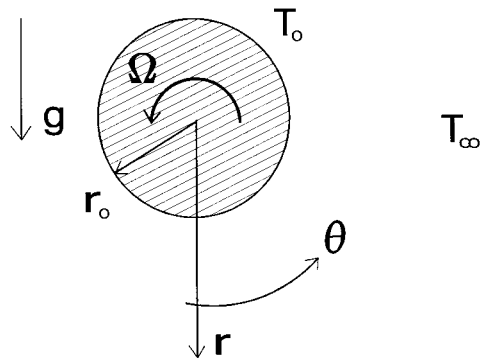

Fig. 1. Schematic of the cylinder and the main physical parameters.

$$u\frac{\partial T}{\partial r}+\frac{v}{r}\frac{\partial T}{\partial \theta}=\alpha\left[\frac{\partial^2 T}{\partial r^2}+\frac{1}{r}\frac{\partial T}{\partial r}+\frac{1}{r^2}\frac{\partial^2 T}{\partial \theta^2}\right]. \tag{4}$$

Eqs. (1)–(4) are subject to the following boundary conditions:

1. On the cylinder surface, $r=r_o$: $u=0$, $v=\Omega r_o$, and $T=T_o$.
2. Far away from the cylinder, $r\to\infty$: $u=v=0$ and $T=T_\infty$.

The average Nusselt number based on diameter ($\overline{Nu_D}$) is calculated as:

$$\overline{Nu_D}\equiv\frac{1}{2\pi}\frac{D}{k}\int_0^{2\pi}h(\theta)\,d\theta$$

$$=-\frac{D}{2\pi(T_o-T_\infty)}\int_0^{2\pi}\frac{\partial T(r_o,\theta)}{\partial r}\,d\theta. \tag{5}$$

The following non-dimensional groups are introduced:

$$R=\frac{r}{r_o},\quad U=\frac{u}{\Omega r_o},\quad V=\frac{v}{\Omega r_o},\quad \phi=\frac{T-T_\infty}{T_o-T_\infty},$$

$$P=\frac{p-p_\infty}{0.5\rho(\Omega r_o)^2}.$$

Using the stream function–vorticity formulation, the non-dimensional form of Eqs. (1)–(4) is given by:

$$\omega=\nabla^2\psi \tag{6}$$

$$U\frac{\partial\omega}{\partial R}+\frac{V}{R}\frac{\partial\omega}{\partial\theta}=\frac{1}{Re}\nabla^2\omega - \frac{Gr}{Re^2}\left[\sin(\theta)\frac{\partial\phi}{\partial R}+\frac{1}{R}\cos(\theta)\frac{\partial\phi}{\partial\theta}\right] \tag{7}$$

$$U\frac{\partial\phi}{\partial R}+\frac{V}{R}\frac{\partial\phi}{\partial\theta}=\frac{1}{RePr}\nabla^2\phi \tag{8}$$

where

$$U=\frac{1}{R}\frac{\partial\psi}{\partial\theta},\quad V=-\frac{\partial\psi}{\partial R}.$$

The new non-dimensional boundary conditions for Eqs. (6)–(8) are given by:

1. On the cylinder surface, $R=1$: $\partial\psi/\partial\theta=0$, $\partial\psi/\partial R=1$, $\omega=\partial^2\psi/\partial R^2$, and $\phi=1$.
2. Faraway from the cylinder, $R\to\infty$: $\partial\psi/\partial\theta=\partial\psi/\partial R=\omega=\phi=0$.

In order to accurately resolve the boundary layer around a cylinder, a grid with small radial spacing is

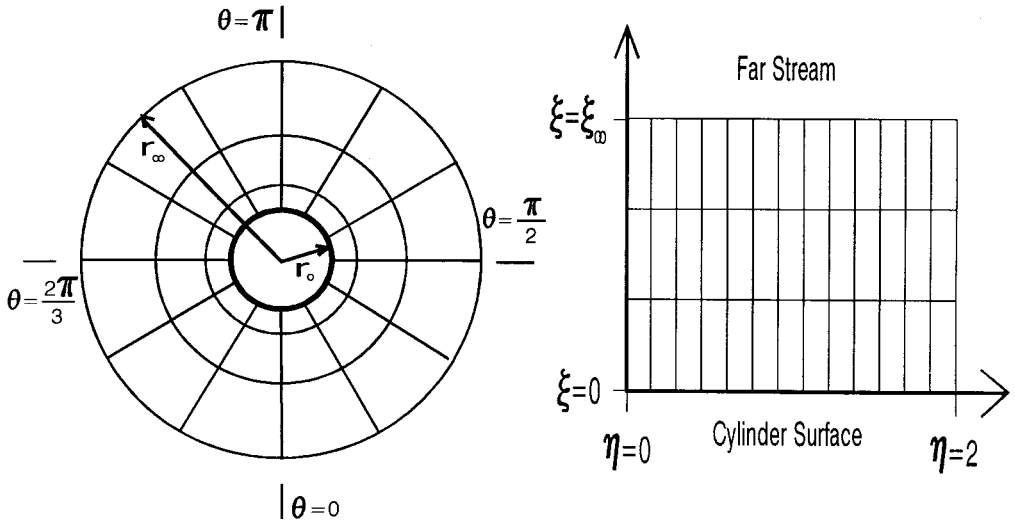

Fig. 2. Schematic of the physical (left) and computational (right) grids.

required. It is not practical to use this small spacing as we move to the far away boundary. Thus a stretched grid in the radial direction is used [16]. This will result in unequally spaced nodes and would require the use of more complicated and/or less accurate finite difference formulas. To overcome this problem, the unequally spaced grid in the physical domain (R, θ) is transformed into an equally spaced grid in the computational domain (ξ, η) [17], see Fig. 2. The two domains are related as follows:

$$R = e^{\pi\xi}, \quad \theta = \pi\eta$$

Eqs. (6)–(8) along with the corresponding boundary conditions need to be transformed into the computational domain. In the new computational domain, the current problem is given by:

$$\omega = \frac{1}{E^2}\left[\frac{\partial^2\psi}{\partial\xi^2} + \frac{\partial^2\psi}{\partial\eta^2}\right] \tag{9}$$

$$\frac{\partial^2\omega}{\partial\xi^2} + \frac{\partial^2\omega}{\partial\eta^2} = Re\left[\frac{\partial\psi}{\partial\eta}\frac{\partial\omega}{\partial\xi} - \frac{\partial\psi}{\partial\xi}\frac{\partial\omega}{\partial\eta}\right] + E\frac{Gr}{Re}\left[\sin(\pi\eta)\frac{\partial\phi}{\partial\xi} + \cos(\pi\eta)\frac{\partial\phi}{\partial\eta}\right] \tag{10}$$

$$\frac{\partial^2\phi}{\partial\xi^2} + \frac{\partial^2\phi}{\partial\eta^2} = \frac{1}{RePr}\left[\frac{\partial\psi}{\partial\eta}\frac{\partial\phi}{\partial\xi} - \frac{\partial\psi}{\partial\xi}\frac{\partial\phi}{\partial\eta}\right] \tag{11}$$

where

$$E = \pi e^{\pi\xi}.$$

The transformed boundary conditions are given by:

1. On the cylinder surface, $\xi = 0$: $\partial\psi/\partial\eta = 0$, $\partial\psi/\partial\xi = -\pi$, $\omega = (1/\pi^2)\partial^2\psi/\partial\xi^2$, and $\phi = 1$.
2. Faraway from the cylinder, $\xi \to \infty$: $\partial\psi/\partial\eta = \partial\psi/\partial\xi = \omega = \phi = 0$.

The elliptic system of PDEs given by Eqs. (9)–(11) along with the corresponding boundary conditions was discretized using the finite difference method. The resulting system of algebraic equations was solved using an explicit hybrid scheme [15]. Such a method proved to be numerically stable for convective-diffusion problems. The finite difference form of the equations was checked for consistency with the original PDEs [16]. The iterative solution procedure was carried out until the error in all solution variables (ψ, ω, ϕ) became less than a predefined error level (ϵ). Other predefined parameters needed for the solution method included the placement of the far away boundary (R_∞) and the number of grid points in both radial and tangential directions, N and M, respectively. Extensive testing was carried out in order to determine the effect of each of these parameters on the solution. This was done to insure that the solution obtained was independent of and not tainted by the predefined value of each of these parameters. The testing included varying the value of ϵ from 10^{-3} to 10^{-6}, R_∞ from 10 to 30, N from 20 to 120, and M from 24 to 144. The results reported herein are based on the following combination: $N = 100$, $M = 100$, $R_\infty = 20$, and $\epsilon = 10^{-5}$.

The first task in any numerical work is to validate

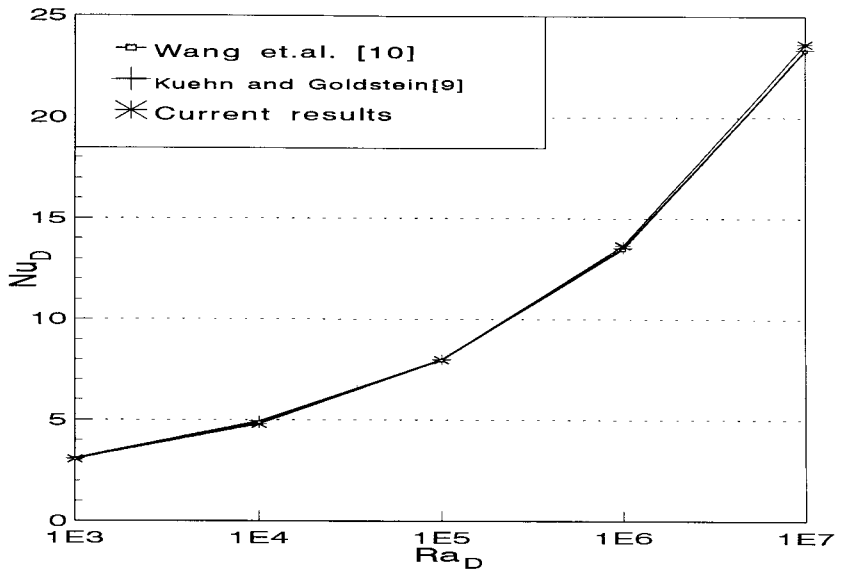

Fig. 3. Variation of the average Nusselt number with Rayleigh number. The case of pure natural convection ($Re_D = 0$).

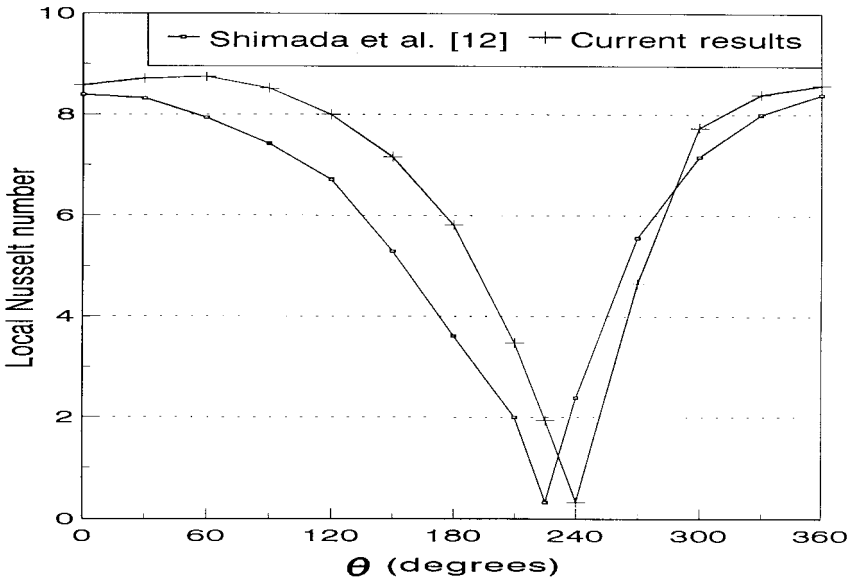

Fig. 4. Variation of the local Nusselt number for the case of $Re_D = 200$ and $\kappa = 1.88$.

the codes ability to accurately reproduce published results. The case of pure natural convection, $Re_D = 0$, was used as an initial test of the code. Fig. 3 shows the average Nusselt number ($\overline{Nu_D}$) at different values of Rayleigh number (Ra_D) as reported by Kuehn and Goldstein [9], Wang et al. [10], and the results of the current code. The current results show excellent agreement with the published data. Only one case could be located in the open literature for a low Reynolds number that is within the range of the current study, the case of $Re_D = 300$ and $\kappa = 1.88$ [12]. Fig. 4 shows a comparison between the experimental local Nusselt number (Nu_D) as reported by Shimada et al. [12] and the numerical predictions of the current code for the case of $Re_D = 300$ and $\kappa = 1.88$. There is a slight shift in the tangential direction between the experimental data and the numerical prediction but the overall behavior and levels are comparable. One cause for the difference is that the experimental data shown in figure 4 read off the figure in the paper by Shimada et al. [12]. Thus, some error is expected due to the resolution of the figure. Another cause could be that the experimental data reported were measured using optical techniques, a Mach–Zehnder interferometer, which does not have a very fine resolution especially near the surface of the cylinder. The procedure used in this code is based on the experience gained in writing another, somewhat more complicated, code that estimates the Nusselt number due to mixed convection from a stationary cylinder in cross flow at different angles of attack. The results of that code showed excellent agreement between published data and numerical predictions over a wide range of Reynolds number, buoyancy parameter, and incoming flow angle of attack [17]. Thus the authors have confidence in the code's ability to accurately predict the current flow field.

The non-dimensional form of the local entropy generation in 2-D cylindrical coordinates is given by [18]:

$$S'''_{gen} = \left[\frac{\nu^2 Gr}{\phi(\nu^2 Gr + T_\infty g\beta r_o^3)}\right]^2 \left[\left(\frac{\partial \phi}{\partial R}\right)^2 + \left(\frac{1}{R}\frac{\partial \phi}{\partial \theta}\right)^2\right] + \frac{g\beta\mu r_o^5\Omega^2}{k(g\beta r_o^3 T_\infty + \nu^2 Gr\phi)} \times \left\{2\left[\left(\frac{\partial U}{\partial R}\right)^2 + \frac{1}{R^2}\left(\frac{\partial V}{\partial \theta} + U\right)^2\right] + \left[\frac{1}{R}\frac{\partial U}{\partial \theta} + R\frac{\partial}{\partial R}\left(\frac{V}{R}\right)\right]^2\right\} \quad (12)$$

where

$$S'''_{gen} = \frac{s'''_{gen} r_o^2}{k}.$$

The total entropy generation is calculated by integrating Eq. (12) over the entire domain as follows:

$$S_t = \int_0^{2\pi}\int_1^{R_\infty} S'''_{gen}(R,\theta) R\, dR\, d\theta. \quad (13)$$

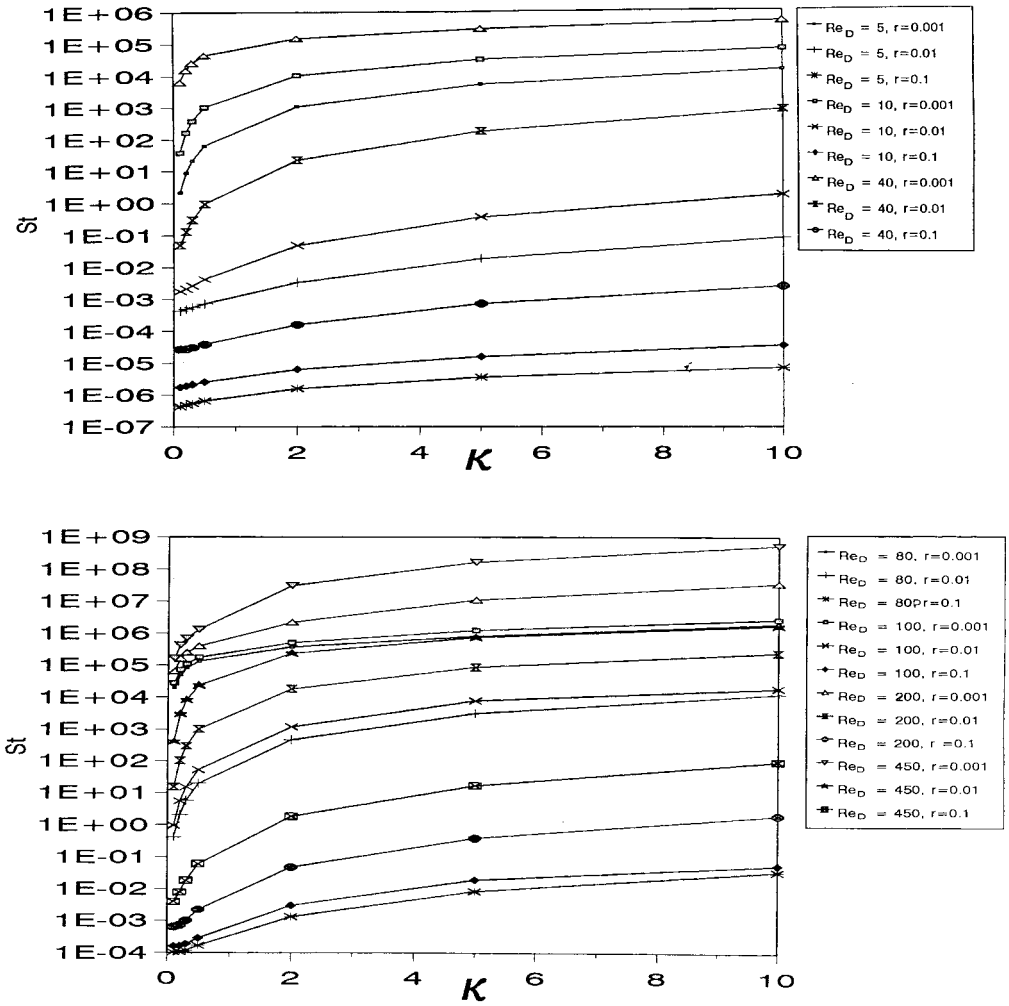

Fig. 5. Variation of the total entropy generation due to buoyancy parameter at different values of Reynolds number and cylinder radius.

The entropy equation consists of two parts, the first is due to conduction while the second is due to viscous dissipation. Entropy generation is calculated after the numerical solution for the velocity and temperature profiles has converged. Thus, Eqs. (12) and (13) need not be written in the stream function–vorticity form nor transformed into the computational domain.

3. Results

The velocity and temperature profiles can be solved analytically for the case of $\kappa = 0$. For this case the radial velocity vanishes ($u = 0$) and the problem becomes independent of the tangential direction (θ). The equation of local entropy generation, Eq. (12), is simplified to:

$$S'''_{\text{gen}} = \frac{4\mu r_o^2 \Omega^2}{kT_\infty}\left(\frac{1}{R^4}\right) \tag{14}$$

The total entropy generation over the entire domain is integrated analytically to get:

$$S_t = 0.3332916\frac{\mu\nu^2 Re^2}{kT_\infty r_o^2} \tag{15}$$

Fig. 5 shows that the total entropy generation increases with both Reynolds number and buoyancy parameter. Higher values of Re_D and/or κ result in smaller viscous and thermal boundary layers. This

translates to higher velocity and temperature gradients and thus, higher rates of entropy generation, Eq. (12). The sharpest rise in the rate of entropy generation occurred at low values of κ. The increase in entropy generation with κ continued up to a certain value of κ then became constant. The value of κ at which the entropy generation became constant depends on Re_D and r_o. This is an important issue from a design point of view. Higher values of κ will result in increased heat transfer from the cylinder, a desired effect in heat exchangers, but usually at the expense of higher entropy generation, i.e. lower thermodynamic efficiency. Fig. 5 shows that the use of very high values of κ results in minimal increase in entropy generation. Thus, higher heat transfer rates can be achieved without the penalty of lower efficiency. Also from Fig. 5, we conclude that the total entropy generation decreases with increasing cylinder radius. Increasing the cylinder radius results in smaller velocity and temperature gradients, for the same value of Reynolds number and buoyancy parameter. Thus, the rate of entropy generation will decrease, Eq. (12).

Fig. 6 shows the change in the contribution of the conduction (S_c) and viscous (S_v) parts to the total

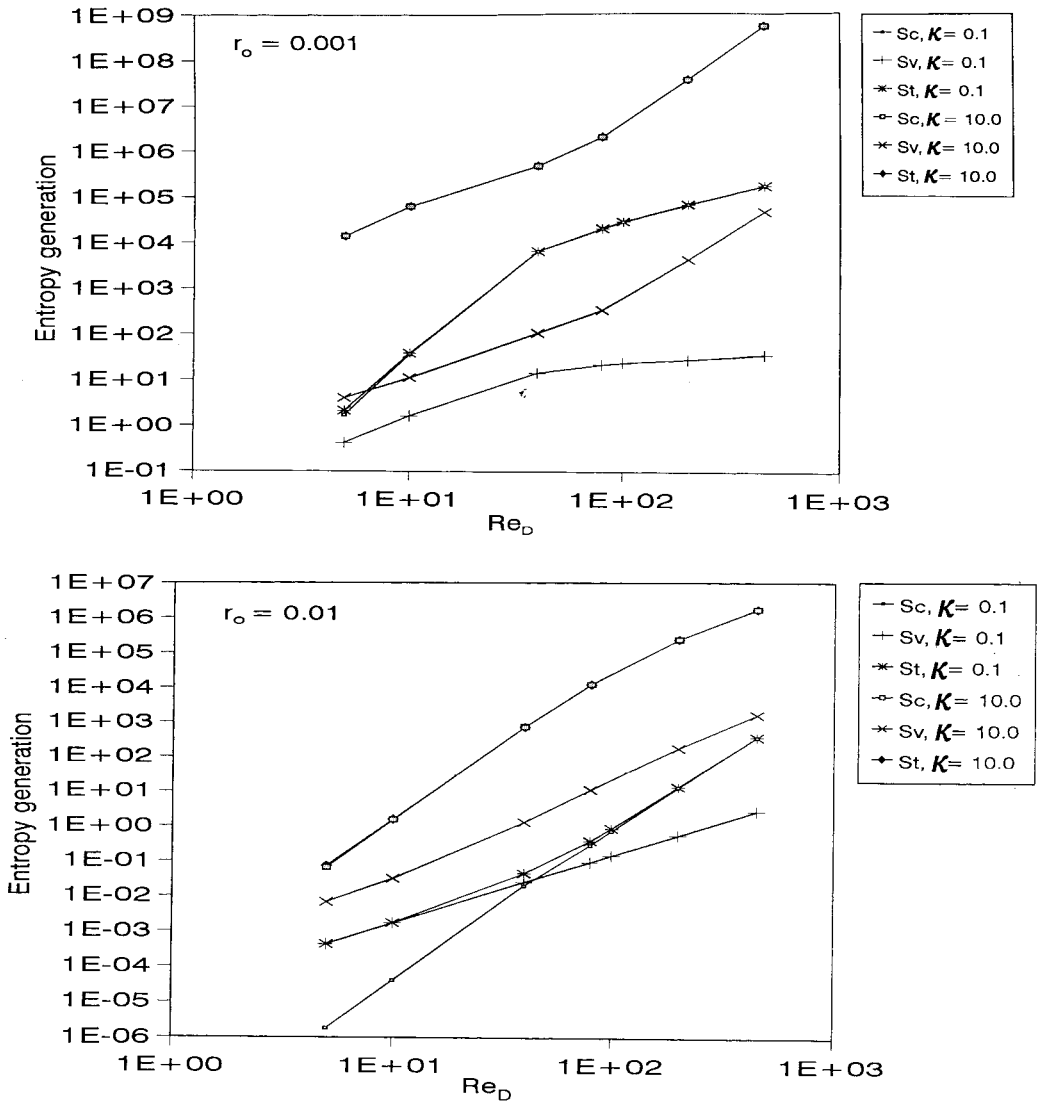

Fig. 6. Conduction, viscous, and total entropy generation at different combinations of Reynolds number, buoyancy parameter, and cylinder radius.

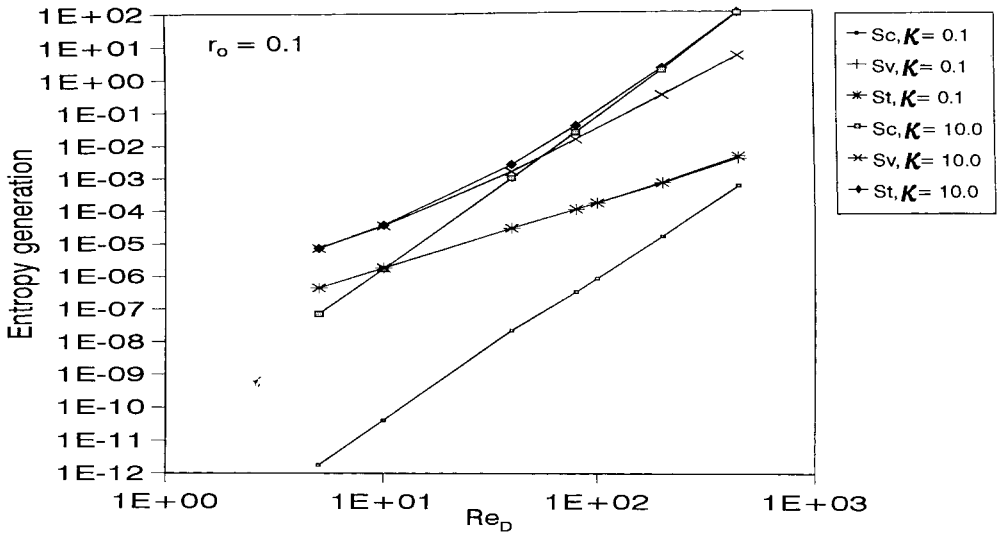

Fig. 6 (*continued*)

entropy generation (S_t) as a function of Reynolds number, buoyancy parameter, and cylinder radius. Knowing which effect is dominant in the total entropy generation is an important issue when trying to devise methods of reducing entropy in order to enhance the thermodynamic efficiencies of thermal systems. The main conclusions of Fig. 6 are:

1. Entropy generation due to conduction effect is dominant at small cylinder radius ($r_o = 0.001$ m), irrespective of the Reynolds number and buoyancy parameter.
2. Entropy generation due to conduction effect is dominant at medium cylinder radius ($r_o = 0.01$ m), except at the combination of low Reynolds number and buoyancy parameter, where the viscous contribution becomes dominant.
3. Entropy generation due to viscous effect is dominant at large cylinder radius ($r_o = 0.1$ m), except at

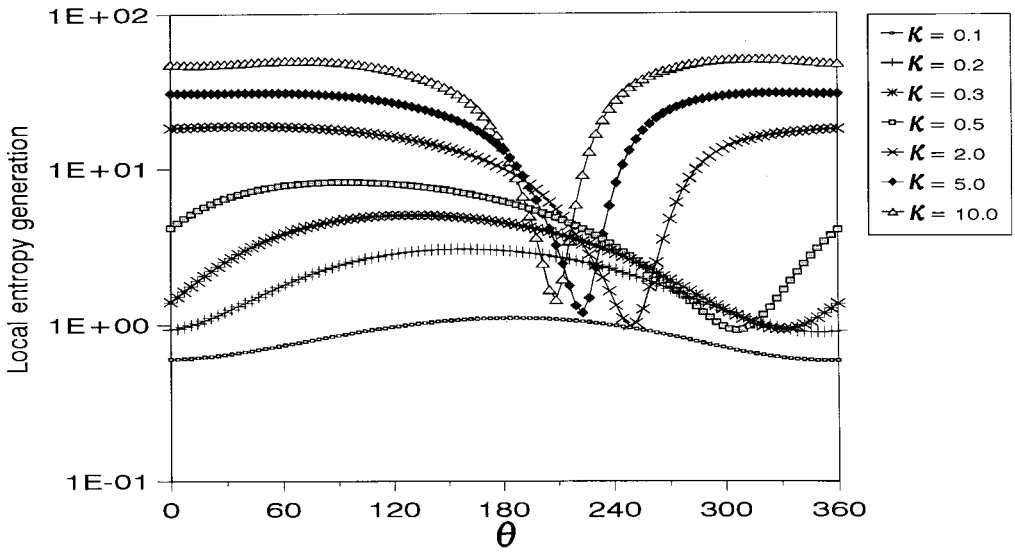

Fig. 7. Variation of the local entropy generation on the cylinder surface due to buoyancy parameter for the case of $Re_D = 200$ and $r_o = 0.001$ m.

the combination of high Reynolds number and buoyancy parameter, where the conduction contribution becomes dominant.

The variation of the local entropy generation around the cylinder as a function of buoyancy parameter is shown in Fig. 7 for the case of $Re_D = 200$ and $r_o = 0.001$ m. This is a representative case for all other cases studied in this research. The only difference between the different cases was the relative reduction in the entropy generation in the plume region. Fig. 7 shows that as the buoyancy parameter increases, the local entropy generation around the cylinder becomes less uniform. Local entropy generation is lowest in the plume region where the velocity and temperature gradients are lowest. Thus, the locus of the minimum local entropy generation in Fig. 7 shows the change in the location of the plume as a function of the buoyancy parameter. As the buoyancy parameter increases, the flow approaches the case of pure natural convection. Indeed, at $\kappa = 10$, the plume is around $\theta = 210^\circ$.

4. Conclusions

Entropy generation due to natural convection from a rotating cylinder was calculated numerically. The results show that the total entropy generation increases with the increase of both Reynolds number and buoyancy parameter but decreases as the cylinder radius increases. The change in total entropy generation with buoyancy parameter reaches an asymptotic value beyond which entropy generation does not increase with further increases in the buoyancy parameter. The relative contribution of the two parts of entropy generation was mainly a function of the cylinder radius and, to a lesser extent, a function of Reynolds number and buoyancy parameter. These results are an important first step in the quest to devise methods for the reduction of entropy generation in order to enhance the thermodynamic efficiency of thermal systems.

References

[1] A. Bejan, A study of entropy generation in fundamental convective heat transfer, J. Heat Transfer 101 (1979) 718–727.
[2] J.Y. San, Z. Laven, Entropy generation in convective heat transfer and isothermal convective mass transfer, J. Heat Transfer 109 (1987) 647–652.
[3] R.A. Hutchinson, S.E. Lyke, Microcomputer analysis of regenerative heat exchangers for oscillating flows, in: Proceedings of the Second ASME/JSME Thermal Engineering Joint Conference, 1987, pp. 653–663.
[4] A. Bejan, The concept of irreversibility in heat exchanger design counter flow heat exchangers for gas-to-gas applications, J. Heat Transfer 99 (1977) 334–380.
[5] C.H. Cheng, W.H. Huang, Entropy generation and heat transfer via laminar forced convection channel flows over transverse fins in entrance region, Applied Energy 32 (1989) 241–267.
[6] C.H. Cheng, W.P. Ma, Numerical prediction of entropy generation for mixed convection flows in a vertical channel with transverse fins arrays, Int. Comm. In Heat and Mass Transfer 21 (1994) 519–530.
[7] M.K. Drost, M.D. White, Numerical prediction of local entropy generation in an impinging jet, J. Heat Transfer 113 (1991) 823–829.
[8] Desederi, Umberto, Bindi, Giani, Minimizing entropy generation to optimize the heat transfer of heat recovery boiler in combined cycle power plant, Int. Gas Turbine Institute 8 (1993) 427–434.
[9] T.H. Kuehn, R.J. Goldstein, Numerical solution to the Navier–Stokes equations for laminar natural convection about a horizontal isothermal circular cylinder, Int. J. Heat Mass Transfer 23 (1980) 971–979.
[10] P. Wang, R. Kahawita, T.H. Nguyen, Numerical computation of the natural convection flow about a horizontal cylinder using splines, Numerical Heat Transfer 17 (1990) 191–215.
[11] N.K. Ghaddar, F. Thiele, Natural convection over a rotating cylindrical heat source in a rectangular enclosure, Numerical Heat Transfer 26 (1994) 701–717.
[12] R. Shimada, T. Ohkubo, T. Kobayashi, S. Kumagi, Heat transfer from a rotating cylinder with and without cross flow, Trans. JSME 57 (1991) 210–216.
[13] H.M. Badr, A theoretical study of laminar mixed convection from a horizontal cylinder in a cross stream, Int. J. Heat Mass Transfer 26 (1983) 639–653.
[14] H.M. Badr, S.C.R. Dennis, P.J.S. Young, Steady and unsteady flow past a rotating circular cylinder at low Reynolds numbers, Computers & Fluids 17 (1989) 579–609.
[15] R.A. Ahmad, Steady-state numerical solution of the Navier–Stokes and energy equations around a horizontal cylinder at moderate Reynolds numbers from 100–500, Heat Transfer Engineering 17 (1996) 31–81.
[16] J.D. Anderson, Computational Fluid Dynamics: The Basics with Applications, McGraw Hill, New York, 1994.
[17] B.A./K. Abu-Hijleh, Laminar mixed convection correlations for an isothermal cylinder in cross flow at different angles of attack, Int. J. Heat and Mass Transfer (1990) 42 1383–1388.
[18] A. Bejan, Entropy Generation Through Heat and Fluid Flow, Wiley Interscience, New York, 1994.